JOURNAL OF GUIDANCE, CONTROL, AND DYNAMICS
Vol. 18, No. 3, May–June 1995

Autonomous Orbit and Magnetic Field Determination Using Magnetometer and Star Sensor Data

Mark L. Psiaki*
Cornell University, Ithaca, New York 14853-7501

A batch filter has been adapted to autonomously determine spacecraft orbit and corrections to Earth's magnetic field model. It uses only magnetometer and star sensor measurements. This filter's aim is to improve the accuracy of magnetometer-based spacecraft orbit determination. Observability of the system is demonstrated through covariance analysis. The results of filtering data from a truth model simulation predict the method's accuracy. The truth model includes random magnetometer noise, random star sensor attitude errors, and high-spatial- frequency magnetic field uncertainties. System accuracy is highest for low altitude, about 500 km, and significant inclination, 45 deg or larger. Accuracies on the order of 200 m for position and 1 nT for field model coefficients are predicted by the study. The only unobservable situation is that of an orbit with zero inclination and zero eccentricity, but accuracy degrades markedly for nearly circular orbits with low inclination.

I. Introduction

KNOWLEDGE of spacecraft position and orbit is a practical operational requirement for most missions. The objective of the present study is to explore a novel way of determining a low Earth-orbiting spacecraft's orbit. This technique requires only magnetic field measurements from a three-axis magnetometer and three-axis attitude measurements derived from star sensors. The technique passes a time series of such measurements through a nonlinear least-squares batch filter to simultaneously estimate the orbit, magnetometer biases, and corrections to a model of Earth's magnetic field.

Such a system could be used for autonomous spacecraft navigation, given enough on-board computer power. Additionally, the method could be used by geomagnetism researchers to lower the costs of space-based surveys of Earth's magnetic field: the need for an independent spacecraft tracking system could be eliminated. The technique also could be used for orbit/field determinations for low planetary orbiters on missions to planets with strong magnetic fields (e.g., Jupiter, Saturn, and Uranus[1]).

Admittedly, the proposed system has some economic disadvantages. First, spacecraft that have sensors with the required levels of accuracy are likely to have more stringent position determination requirements than can be achieved by the proposed system. Second, although the proposed system's accuracy may be sufficient for back-up mode operation, its complexity militates against its use as a back-up system.

Even if the proposed system never gets used, the present study is useful because it could point the way to the study of less costly systems. If the proposed system looks promising technically, similar results may be achievable by using a similar filter with a less costly compliment of sensors: a sun sensor, a horizon scanner, and a magnetometer. If, on the other hand, the present study shows poor performance, then there is little hope of achieving useful results with other sensor compliments that derive position information from Earth's magnetic field.

The main emphasis of the current paper is to demonstrate the practical observability of the orbit and the magnetic field model given roughly a day's worth of sensor measurements sampled almost continuously. Practical observability needs to be demonstrated because the system is so unusual: Its only means of getting the spacecraft's Earth-relative position is to measure Earth's magnetic field, yet the filter also tries to estimate corrections to the field model because a priori information about the field is inaccurate.

Orbit determination techniques have been around since the time of Kepler. Most modern nonautonomous techniques for Earth orbiters rely on radio-signal-derived range and range rate measurements and batch least-squares filtering to determine orbits.[2] A number of autonomous techniques have been proposed, and some have been tested.[3–6]

The present idea is an attempt to improve the orbit determination accuracy of the autonomous system tested by Psiaki et al.[5] That system relies solely on measurements from a three-axis magnetometer to determine spacecraft position and orbit. It uses a model of Earth's magnetic field and a model of the orbital dynamics to predict the time-varying magnitude of Earth's magnetic field vector at the spacecraft. The time history of this predicted magnitude is compared with the measured magnitude time history after estimated magnetometer biases are removed. In one version of the scheme, discrepancies between these two time histories are used by a batch filter to improve estimates of the orbit, a drag parameter, and the magnetometer biases.

Reference 6 presents related magnetometer-based autonomous orbit determination schemes and tests them using real flight data. Its systems use extended Kalman filters. One filter uses only the field magnitude, as in Ref. 5, and another includes three-axis attitude information such as would be available from a star sensor system. Accuracies on the order of 10–40 km have been achieved for the Earth Radiation Budget Satellite (ERBS) and Gamma Ray Observatory (GRO) spacecraft.

Reference 5 also tests its scheme on real flight data. Its batch filter has achieved an accuracy of about 8 km peak error operating on data from the Geomagnetic Field Satellite (MAGSAT) and 18 km peak error operating on data from the Dynamics Explorer-2 (DE-2) spacecraft. Although much of the error on the MAGSAT case may have been due to the crudeness of the orbital dynamics model used, the increased error for the DE-2 case is probably due to degraded accuracy in the model used for Earth's magnetic field.

The present scheme addresses the issue of degraded field model accuracy by attempting to estimate the field. Star sensors have been added to the system in hopes of making the orbit and Earth's magnetic field simultaneously observable. Measurements of the field alone, without a celestial attitude reference, would leave unobservable any simultaneous shifts of the orbit and Earth's field in the longitude direction. As is shown below, the addition of three-axis star sensor measurements makes any perturbations of Earth's field observable if the orbit is inclined or noncircular.

Section II of this paper describes the batch filter's structure, including dynamics and measurement models. Section III describes

Received Jan. 28, 1993; presented as Paper 93-3825 at the AIAA Guidance, Navigation, and Control Conference, Monterey, CA, Aug. 9–11, 1993; revision received June 6, 1994; accepted for publication July 20, 1994.

*Associate Professor, Department of Mechanical and Aerospace Engineering. Member AIAA.

a truth model that has been used to generate simulated magnetometer and attitude data for input to the batch filter. Section IV briefly discusses the filter evaluation techniques. These are used in Sec. V to present results that assess the accuracy obtainable by this technique.

II. Batch Filter Structure

A. Estimation Vector Definition

The quantities that get estimated by the batch filter are formed into the estimation vector:

$$\boldsymbol{p} = \Big[\big(M_0, M_1, M_2, e, \omega_0, \lambda_0, i, b_x, b_y, b_z,$$
$$q_1^0, q_1^1, s_1^1, \dot{q}_1^0, \dot{q}_1^1, \dot{s}_1^1, g_1^0, g_1^1, h_1^1,$$
$$\Delta g_1^0, \Delta g_1^1, \Delta h_1^1, \Delta g_2^0, \Delta g_2^1, \Delta h_2^1, \Delta g_2^2,$$
$$\Delta h_2^2, \Delta g_3^0, \ldots, \Delta h_N^N\big)\Big]^T \tag{1}$$

The first seven elements of this vector define the orbit, the position, and a drag term in terms of Kepler elements. They are the same first seven elements as are used in the batch filter of Ref. 5. The quantity M_0 is the mean anomaly at epoch, M_1 the mean motion at epoch, M_2 half the first time derivative of the mean motion (assumed constant over the interval of concern), e the eccentricity, ω_0 the argument of perigee at epoch, λ_0 the longitude of the ascending node at epoch, and i the inclination. The quantity M_2 is an approximate way of including drag effects. Elements 8–10 of $\boldsymbol{p}$, b_x, b_y, and b_z, are the biases on each channel of the magnetometer, just as in the batch filter of Ref. 5.

The latter elements of $\boldsymbol{p}$, $q_1^0, \ldots, \Delta h_N^N$, quantify two types of magnetic field perturbation: an external field caused by a ring current and uncertainty in Earth's main field. Langel[7] discusses mathematical models of Earth's main field and of the external ring current. The notation used here corresponds to his notation. Elements 11–13 of $\boldsymbol{p}$, q_1^0, q_1^1, and s_1^1, give the spherical harmonic coefficients of a first-degree model of the external ring current at epoch, and elements 14–16 of $\boldsymbol{p}$, the terms $\dot{q}_1^0$, $\dot{q}_1^1$, and $\dot{s}_1^1$, model the ring current's time variation as having a constant rate of change. Elements 17–19 of $\boldsymbol{p}$, $\dot{g}_1^0$, $\dot{g}_1^1$, and $\dot{h}_1^1$, model a constant rate of change of the internal field's first-degree coefficients. The ring current induces perturbations to the internal field, and the time-varying nature of the ring current implies time variation of the internal field.

The remaining elements of $\boldsymbol{p}$, $\Delta g_1^0, \ldots, \Delta h_N^N$, are constant perturbations to the coefficients of an Nth-degree, Nth-order spherical harmonic model of Earth's main internal magnetic field, plus induced effects, at epoch. These terms represent perturbations from the 1985 International Geomagnetic Reference Field (IGRF) (Ref. 7, pp. 348–349). Spherical harmonic expansions define the field in terms of IGRF coefficients and these estimation parameters. The expansions are given in Sec. II.C of this paper.

The total number of elements of the $\boldsymbol{p}$ estimation vector is $19 + N^2 + 2N$. For many of the cases considered in Sec. V, $N = 10$ is used for a 10th-degree, 10th-order model of Earth's magnetic field. This yields a 139-element $\boldsymbol{p}$ vector.

B. Orbital Dynamics Model

The orbital dynamics model provides a way of determining the spacecraft position at any given time since epoch, Δt, based on the first seven elements of the $\boldsymbol{p}$ estimation vector. Position is needed by the filter to determine the expected magnetic field, a function of position, at each measurement instant. The filter's orbital dynamics model takes the form

$$\theta = \theta(\Delta t;\, M_0,\, M_1,\, M_2,\, e,\, \omega_0,\, \lambda_0,\, i) \tag{2a}$$

$$\phi = \phi(\Delta t;\, M_0,\, M_1,\, M_2,\, e,\, \omega_0,\, \lambda_0,\, i) \tag{2b}$$

$$r = r(\Delta t;\, M_0,\, M_1,\, M_2,\, e,\, \omega_0,\, \lambda_0,\, i) \tag{2c}$$

where θ is the colatitude, ϕ the longitude, and r the geocentric radius. The formulas for these three functions are given in the Appendix. They are based on Kepler's laws with secular J_2 and drag perturbations.

The dynamic model used in this study can have an inaccuracy on the order of 10 km for one day's worth of position propagations. The results of this paper show the possibility of achieving much better positional accuracy with the orbit determination scheme proposed here. Such optimistic results are possible because the dynamic model assumed in the truth model is identical to the model used in the filter. When working with real spacecraft data, however, a much better dynamic model would be needed in order for the filter to achieve the accuracies reported below. The crude model used here has been adopted only to expedite the process of demonstrating the practical observability of the proposed system.

C. Measurement Model

The system uses local measurements of Earth's magnetic field in spacecraft coordinates, $\boldsymbol{B}_{\text{meas}}$, along with measurements of the spacecraft's attitude. The attitude must be measured with respect to inertial coordinates, Earth-centered celestial coordinate system in this case: X in the equatorial plane and pointing toward the first point of Aries, Z along the north pole, and Y in the equatorial plane and defined by the right-hand rule. For a given time since epoch, the spacecraft's measured celestial attitude is given in terms of the transformation matrix from celestial coordinates (cc) to spacecraft coordinates (sc), $A_{\text{sc/cc}_{\text{meas}}}(\Delta t)$.

Another quantity available to the filter is the Greenwich hour angle of the first point of Aries at epoch, γ_0. It is the angle between the first point of Aries and the intersection of the Greenwich meridian with the equator. It can be computed from the Universal time at epoch.

The batch filter needs to compute an estimate of what $\boldsymbol{B}_{\text{meas}}$ should be, denoted as $\boldsymbol{B}_{\text{mod}}$, at each sample time Δt. It can be calculated given Δt, $\boldsymbol{A}_{\text{sc/cc}_{\text{meas}}}(\Delta t)$, γ_0, and $\boldsymbol{p}$, the estimation vector. The calculation begins by using Δt and the first seven elements of $\boldsymbol{p}$ to compute estimates of $\theta(\Delta t)$, $\phi(\Delta t)$, and $r(\Delta t)$ using the equations in the Appendix. Next, the procedure uses the spherical harmonic model of Ref. 7 to calculate the estimated magnetic field in local south, east, and zenith coordinates:

$$B_\theta = -\Bigg[\left(q_1^0 + \dot{q}_1^0\,\Delta t\right) + \left(\frac{a}{r}\right)^3\left(g_1^0 + \Delta g_1^0 + \dot{g}_1^0\,\Delta t\right)\Bigg]$$
$$\times \frac{\mathrm{d}P_1^0(\cos\theta)}{\mathrm{d}\theta} - \Bigg\{\left(q_1^1 + \dot{q}_1^1\,\Delta t\right)\cos\phi + \left(s_1^1 + \dot{s}_1^1\Delta t\right)\sin\phi$$
$$+ \left(\frac{a}{r}\right)^3\Big[\left(g_1^1 + \Delta g_1^1 + \dot{g}_1^1\Delta t\right)\cos\phi$$
$$+ \left(h_1^1 + \Delta h_1^1 + \dot{h}_1^1\,\Delta t\right)\sin\phi\Big]\Bigg\}\frac{\mathrm{d}P_1^1(\cos\theta)}{\mathrm{d}\theta}$$
$$- \sum_{n=2}^{N}\left(\frac{a}{r}\right)^{n+2}\sum_{m=0}^{n}\Big\{\left(g_n^m + \Delta g_n^m\right)\cos m\phi$$
$$+ \left(h_n^m + \Delta h_n^m\right)\sin m\phi\Big\}\frac{\mathrm{d}P_n^m(\cos\theta)}{\mathrm{d}\theta} \tag{3a}$$

$$B\phi = \frac{1}{\sin\theta}\Bigg(\Bigg\{\left(q_1^1 + \dot{q}_1^1\,\Delta t\right)\sin\phi - \left(s_1^1 + \dot{s}_1^1\,\Delta t\right)\cos\phi$$
$$+ \left(\frac{a}{r}\right)^3\Big[\left(g_1^1 + \Delta g_1^1 + \dot{g}_1^1\,\Delta t\right)\sin\phi$$
$$- \left(h_1^1 + \Delta h_1^1 + \dot{h}_1^1\,\Delta t\right)\cos\phi\Big]\Bigg\}P_1^1(\cos\theta)$$
$$+ \sum_{n=2}^{N}\left(\frac{a}{r}\right)^{n+2}\sum_{m=0}^{n} m\Big\{\left(g_n^m + \Delta g_n^m\right)\sin m\phi$$
$$- \left(h_n^m + \Delta h_n^m\right)\cos m\phi\Big\}P_n^m(\cos\theta)\Bigg) \tag{3b}$$

$$B_r = \left[-\left(q_1^0 + \dot{q}_1^0\,\Delta t\right) + 2\left(\frac{a}{r}\right)^3\left(g_1^0 + \Delta g_1^0 + \dot{g}_1^0\Delta t\right)\right] \times P_1^0(\cos\theta) + \left\{-\left(q_1^1 + \dot{q}_1^1\,\Delta t\right)\cos\phi - \left(s_1^1 + \dot{s}_1^1\Delta t\right)\sin\phi + 2\left(\frac{a}{r}\right)^3\left[\left(g_1^1 + \Delta g_1^1 + \dot{g}_1^1\Delta t\right)\cos\phi + \left(h_1^1 + \Delta h_1^1 + \dot{h}_1^1\Delta t\right)\sin\phi\right]\right\} P_1^1(\cos\theta) + \sum_{n=2}^{N}(n+1)\left(\frac{a}{r}\right)^{n+2}\sum_{m=0}^{n}\left\{\left(g_n^m + \Delta g_n^m\right)\cos m\phi + \left(h_n^m + \Delta h_n^m\right)\sin m\phi\right\} P_n^m(\cos\theta) \tag{3c}$$

or written in vector form

$$\boldsymbol{B}_{\text{sez}}(\theta,\ \phi,\ r;\ \boldsymbol{p},\ \Delta t) = \begin{bmatrix} B_\theta \\ B_\phi \\ B_r \end{bmatrix} \tag{4}$$

where direct dependence upon $\boldsymbol{p}$ comes through terms such as q_1^0 and Δh_n^m. Note that $\boldsymbol{B}_{\text{sez}}$ also depends on $\boldsymbol{p}$ indirectly through the quantities θ, ϕ, and r. The functions $P_n^m(\cos\theta)$ are Legendre functions of degree n and order m in Schmidt quasinormalized form.[7] The parameter a is Earth's mean radius. (The value $a = 6371.2 \times 10^3$ m is used for the magnetic field model because it is the traditional value used within the international geomagnetism research community for normalization of the field coefficients $g_1^0, g_1^1, h_1^1, \ldots$. Note that Earth oblateness causes it to differ from the equatorial radius used in the orbital dynamics of the Appendix.)

The modeled magnetic field can be transformed from local south-east-zenith coordinates into spacecraft-fixed coordinates given the angles γ_0, θ, and ϕ, the time since epoch Δt, and the transformation matrix $\boldsymbol{A}_{\text{sc/cc}_{\text{meas}}}(\Delta t)$. The quantities γ_0, θ, ϕ, and Δt define the transformation from local south-east-zenith coordinates to celestial coordinates, $\boldsymbol{A}_{\text{cc/sez}}(\gamma_0,\ \theta,\ \phi,\ \Delta t)$. The product $\boldsymbol{A}_{\text{sc/cc}_{\text{meas}}}\boldsymbol{A}_{\text{cc/sez}}$ is the transformation from south-east-zenith coordinates into spacecraft coordinates.

Given the foregoing definitions, the expression for the modeled magnetic field vector, the vector the filter expects to read from the magnetometer at time Δt, is

$$\boldsymbol{B}_{\text{mod}}(\boldsymbol{p},\ \Delta t) = \boldsymbol{A}_{\text{sc/cc}_{\text{meas}}}\boldsymbol{A}_{\text{cc/sez}}(\gamma_0,\ \theta,\ \phi,\ \Delta t) \times \boldsymbol{B}_{\text{sez}}(\theta,\ \phi,\ r;\ \boldsymbol{p},\ \Delta t) + \begin{bmatrix} b_x \\ b_y \\ bz \end{bmatrix} \tag{5}$$

Note that, in addition to the explicit dependence of $\boldsymbol{B}_{\text{mod}}$ on $\boldsymbol{p}$ in Eq. (5), indirect dependence on $\boldsymbol{p}$ comes through θ, ϕ, and r; cf. Eqs. (2a–2c) and the Appendix.

The batch filter needs to know the first partial derivative of $\boldsymbol{B}_{\text{mod}}$ with respect to $\boldsymbol{p}$. This can be computed using the chain rule:

$$\frac{\partial \boldsymbol{B}_{\text{mod}}}{\partial \boldsymbol{p}} = \boldsymbol{A}_{\text{sc/cc}_{\text{meas}}}\left[\left(\frac{\partial \boldsymbol{A}_{\text{cc/sez}}}{\partial\theta}\boldsymbol{B}_{\text{sez}}\right)\frac{\partial\theta}{\partial\boldsymbol{p}} + \left(\frac{\partial \boldsymbol{A}_{\text{cc/sez}}}{\partial\phi}\boldsymbol{B}_{\text{sez}}\right)\frac{\partial\phi}{\partial\boldsymbol{p}} + \boldsymbol{A}_{\text{cc/sez}}\left(\frac{\partial \boldsymbol{B}_{\text{sez}}}{\partial\theta}\frac{\partial\theta}{\partial\boldsymbol{p}} + \frac{\partial \boldsymbol{B}_{\text{sez}}}{\partial\phi}\frac{\partial\phi}{\partial\boldsymbol{p}} + \frac{\partial \boldsymbol{B}_{\text{sez}}}{\partial r}\frac{\partial r}{\partial\boldsymbol{p}} + \frac{\partial \boldsymbol{B}_{\text{sez}}}{\partial\boldsymbol{p}}\right)\right] + \begin{bmatrix} \dfrac{\partial b_x}{\partial\boldsymbol{p}} \\ \dfrac{\partial b_y}{\partial\boldsymbol{p}} \\ \dfrac{\partial b_z}{\partial\boldsymbol{p}} \end{bmatrix} \tag{6}$$

where the last term is a matrix with all zeros except for three entries that equal 1. Computational efficiency can be gained in the calculation of $\boldsymbol{B}_{\text{mod}}$ and its partial derivatives if the Eqs. (3a–3c) series and their partial derivatives are calculated recursively as in Ref. 8.

D. Batch Nonlinear Least-Squares Estimation and Statistical Model

The batch least-squares cost function is the sum of the squares of the errors between the components of the measured field and the modeled field time series in spacecraft coordinates. In order to give the cost function a statistical meaning as a negative likelihood function, the component errors are normalized by the standard deviation of the magnetometer random noise σ_m. This noise is assumed to be Gaussian. Assuming that there are K measurements, $\boldsymbol{B}_{\text{meas}_k}$ for $k = 1, \ldots, K$, at the sample times Δt_k, the least-squares cost function is

$$J(\boldsymbol{p}) = \frac{1}{2\sigma_m^2}\sum_{k=1}^{K}\left[\boldsymbol{B}_{\text{meas}_k} - \boldsymbol{B}_{\text{mod}}(\boldsymbol{p},\ \Delta t_k)\right]^T \times \left[\boldsymbol{B}_{\text{meas}_k} - \boldsymbol{B}_{\text{mod}}(\boldsymbol{p},\ \Delta t_k)\right] \tag{7}$$

The batch filter operates by performing a general nonlinear minimization of this cost function with respect to $\boldsymbol{p}$. It uses the Gauss–Newton method for nonlinear least-squares problems[9] to determine search directions, and it uses restricted-step line searches to ensure descent and robust convergence. This technique is identical to that used in Ref. 5.

The $J(\boldsymbol{p})$ function in Eq. (7) can have multiple local minima. This possibility results from the nonlinearity of the $\boldsymbol{B}_{\text{mod}}(\boldsymbol{p},\ \Delta t)$ function in Eq. (5), which makes $J(\boldsymbol{p})$ nonquadratic in $\boldsymbol{p}$. The Gauss-Newton method could converge to a local minimum of $J(\boldsymbol{p})$ that is very far from the true $\boldsymbol{p}$ vector. The only way to ensure convergence to the correct local minimum is to start the Gauss-Newton minimization with a guess of $\boldsymbol{p}$ that is close to the actual $\boldsymbol{p}$. As discussed below, experience with the current estimation problem suggests that convergence to the correct local minimum can be achieved for initial guesses of $\boldsymbol{p}$ that correspond to rather large initial rms errors in the spacecraft position.

Minimization of this cost function effectively minimizes the 2-norm of the error in the following measurement equations:

$$\frac{1}{\sigma_m}\boldsymbol{B}_{\text{meas}_k} = \frac{1}{\sigma_m}\boldsymbol{B}_{\text{mod}}(\boldsymbol{p},\ \Delta t_k) \qquad \text{for} \qquad k = 1, \ldots, K \tag{8}$$

If random magnetometer measurement noise is the principal cause of any errors in Eq. (8) after minimizing $\boldsymbol{p}$, then these errors will have zero mean and a unit variance, and they will be uncorrelated. In this case, the Jacobian of Eq. (8) with respect to $\boldsymbol{p}$ can be used to calculate the covariance of the estimate of $\boldsymbol{p}$. If the Jacobian matrix is

$$A = \frac{1}{\sigma_m}\begin{bmatrix} \dfrac{\partial \boldsymbol{B}_{\text{mod}}(\boldsymbol{p},\ \Delta t_1)}{\partial\boldsymbol{p}} \\ \dfrac{\partial \boldsymbol{B}_{\text{mod}}(\boldsymbol{p},\ \Delta t_2)}{\partial\boldsymbol{p}} \\ \vdots \\ \dfrac{\partial \boldsymbol{B}_{\text{mod}}(\boldsymbol{p},\ \Delta t_K)}{\partial\boldsymbol{p}} \end{bmatrix} \tag{9}$$

then the covariance of the estimated $\boldsymbol{p}$ is

$$\boldsymbol{P}_p = (\boldsymbol{A}^T\boldsymbol{A})^{-1} \tag{10}$$

III. Truth Model

The truth model generates simulated magnetometer and celestial attitude data for later input to the batch least-squares filter. Also, the truth model has a known actual spacecraft orbit and associated position time history. Comparison of the truth model's position time history with the filter's estimated position time history is a principal means of filter evaluation.

A. Dynamics

The truth model has orbital and attitude dynamics. The orbital motion is modeled using truth model values for M_0, M_1, M_2, e, ω_0, λ_0, and i. These are input to the same position equations as the filter uses [Eqs. (A1–A10c) of the Appendix] to get the truth model position. Like the filter's orbit model, the truth model includes no higher order geopotential effects beyond the secular J_2 effects. As mentioned above, this perfect correspondence between the form of the truth model orbital motion and the form of the filter's orbital model is an unrealistic assumption when working with real flight data. This assumption masks the effects of dynamic model uncertainty on the new method's orbit determination accuracy. Given more sophisticated orbit models such as those used in Ref. 2, however, the dynamics uncertainty effect for real flight data could be reduced to a level of minor significance. Therefore, this simplistic truth model seems justified for purposes of showing practical observability.

The attitude dynamics truth model is rather simple. It assumes that the spacecraft is nadir pointing. For most runs, the spacecraft is assumed to maintain a constant yaw orientation with respect to the orbit normal. The pitch axis remains fixed in spacecraft coordinates, and the inertial angular velocity of the spacecraft approximately equals the orbital rate and is directed along the negative pitch axis, which corresponds to the orbit normal direction. In some unusual cases, the attitude model includes an abrupt 90 deg yaw maneuver before the last orbit of a data batch. This causes the pitch and roll axes to interchange. This maneuver has been used in cases of low orbital inclination to improve the magnetometer pitch axis bias estimate. The attitude dynamics truth model has as its output $\boldsymbol{A}_{\mathrm{sc/cc}}(\Delta t_k)$, the true transformation matrix between celestial coordinates and spacecraft coordinates.

B. Measurement Model

The truth model generates γ_0 and two types of measurement data for a given run: $\boldsymbol{B}_{\mathrm{meas}_k}$ for $k = 1, \ldots, K$ and $\boldsymbol{A}_{\mathrm{sc/cc}_{\mathrm{meas}}}(\Delta t_k)$ for $k = 1, \ldots, K$. The angle γ_0 is provided by the truth model without error.

To generate $\boldsymbol{B}_{\mathrm{meas}_k}$, the truth model uses nonzero "truth" values for the quantities q_1^0, q_1^1, s_1^1, $\dot{q}_1^0$, $\dot{q}_1^1$, $\dot{s}_1^1$, $\dot{g}_1^0$, $\dot{g}_1^1$, $\dot{h}_1^1$, Δg_1^0, Δg_1^1, Δh_1^1, Δg_2^0, Δg_2^1, Δh_2^1, Δg_2^2, Δh_2^2, $\Delta g_3^0, \ldots, \Delta h_N^N$, which define an external time-varying field and perturbations from the 1985 IGRF model of the internal field. Consistent with a period of low magnetic storm activity, the external field (q_1^0, q_1^1, s_1^1, $\dot{q}_1^0$, $\dot{q}_1^1$, and $\dot{s}_1^1$) has been modeled as being aligned with Earth's main dipole field, as being on the order of 10–20 nT in strength and as varying at a rate of about 20 nT/day or less. Similarly, the rates of change of the first-degree internal terms ($\dot{g}_1^0$, $\dot{g}_1^1$, and $\dot{h}_1^1$) have been chosen to be 27% of the corresponding external field coefficient rates of change.[7] The internal field coefficient perturbations ($\Delta g_1^0, \ldots, \Delta h_N^N$) each have been chosen randomly from a zero-mean Gaussian distribution. In most cases reported in Sec. V, the standard deviation of each perturbation's distribution has been set equal to 1% of the magnitude of the corresponding 1985 IGRF coefficient.

The degree of the magnetic model used for the truth model has been chosen to be higher than the degree of the model used in the filter. This is necessary because a significant source of systematic error in the method comes from the need to limit the degree of the field model used in the filter. Earth's true field has infinite degree. Most cases reported in this paper use a 13th-degree field in the truth model and a 10th-degree field in the filter. The 1985 IGRF has terms up to only degree 10. The truth model uses 11th- to 13th-degree coefficients found in Ref. 10. Although these do not correspond to the post-1985 time frame of the 1st- through 10th-degree coefficients, they give a systematic error source due to unmodeled high-spatial-frequency effects, and they have approximately the right magnitude.

The measured magnetic field is computed as follows. For a given sample time Δt_k, the truth model orbit parameters are used in Eqs. (A1–A10c) to compute the truth model spacecraft position, θ_k, ϕ_k, and r_k. Similarly, the attitude dynamics truth model is used to determine $\boldsymbol{A}_{\mathrm{sc/cc}}(\Delta t_k)$. These quantities along with truth model magnetometer biases b_x, b_y, and b_z are used in Eqs. (3a–5) to give a truth model magnetic field vector in spacecraft-fixed coordinates. Truth model biases falling in the range ± 180 nT have been used. After adding a Gaussian, zero-mean random magnetometer noise term to each element of this spacecraft-referenced field vector, it becomes $\boldsymbol{B}_{\mathrm{meas}_k}$. The standard deviation for this noise level, σ_m, has been set at 10 nT for all of the cases studied in this paper, which is three times less accurate than the vector magnetometer used on the MAGSAT spacecraft.[10]

The truth model includes random errors in the determination of the spacecraft's celestial attitude. The truth model transformation matrix $\boldsymbol{A}_{\mathrm{sc/cc}}(\Delta t_k)$ is left multiplied by an attitude error transformation matrix to yield the transformation matrix that is given to the filter, $\boldsymbol{A}_{\mathrm{sc/cc}_{\mathrm{meas}}}(\Delta t_k)$. The attitude error transformation matrix is generated randomly to model a per-axis star sensor measurement error that is Gaussian with a mean of 0 and a standard deviation of 2 arcsec.

IV. Filter Evaluation Techniques

A. Covariance Analysis

Pure mathematical observability of the system can be examined by computing the rank of the Jacobian matrix $\boldsymbol{A}$ defined in Eq. (9). The matrix $\sigma_m^2 \boldsymbol{A}^T \boldsymbol{A}$ is the observability Grammian for the linearization of this system. The linearized system will be observable, which implies local observability of the nonlinear system, if the Grammian is nonsingular. This is equivalent to the requirement that $\boldsymbol{A}$ have full column rank.

The dependence of system observability on the rank of $\boldsymbol{A}$ might tempt one to use the condition number of $\boldsymbol{A}$ as a measure of observability. Unfortunately, the condition number depends on problem scaling, which depends on the choice of variables and units used to define the elements of $\boldsymbol{p}$. Although the condition number of $\boldsymbol{A}$ must be less than infinity for observability to hold, its absolute size is not necessarily a good measure of relative observability.

Observability is more practically quantified by computing the linearized system's covariance matrix $\boldsymbol{P}_p$, as defined in Eq. (10). Mathematical observability must hold for $\boldsymbol{P}_p$ to be finite, and practical observability holds if $\boldsymbol{P}_p$ is small in some reasonable sense.

To determine whether $\boldsymbol{P}_p$ is small in terms of spacecraft position error, it is necessary to derive a related covariance matrix, the position covariance, which is a function of time. One such covariance matrix gives the expected uncertainty levels of θ, ϕ, and r due to the uncertainty levels in $\boldsymbol{p}$ that are expressed in $\boldsymbol{P}_p$. This 3×3 covariance matrix is

$$\boldsymbol{P}_{\theta\phi r}(\Delta t) = \begin{bmatrix} \left.\dfrac{\partial \theta}{\partial \boldsymbol{p}}\right|_{(\Delta t, \boldsymbol{p})} \\ \left.\dfrac{\partial \phi}{\partial \boldsymbol{p}}\right|_{(\Delta t, \boldsymbol{p})} \\ \left.\dfrac{\partial r}{\partial \boldsymbol{p}}\right|_{(\Delta t, \boldsymbol{p})} \end{bmatrix} \boldsymbol{P}_p \begin{bmatrix} \left.\dfrac{\partial \theta}{\partial \boldsymbol{p}}\right|^T_{(\Delta t, \boldsymbol{p})'} & \left.\dfrac{\partial \phi}{\partial \boldsymbol{p}}\right|^T_{(\Delta t, \boldsymbol{p})'} & \left.\dfrac{\partial r}{\partial \boldsymbol{p}}\right|^T_{(\Delta t, \boldsymbol{p})} \end{bmatrix} \tag{11}$$

An alternate 3×3 position covariance matrix gives the position uncertainty levels expressed in terms of the local along-track, cross-track, and altitude directions, which are orbit relative:

$$\boldsymbol{P}_{\mathrm{aca}}(\Delta t) = \boldsymbol{T}(\Delta t; \omega, \nu, i, \lambda, \theta, \phi, r) \times \boldsymbol{P}_{\theta\phi r}(\Delta t) \boldsymbol{T}^T(\Delta t; \omega, \nu, i, \lambda, \theta, \phi, r) \tag{12}$$

where the 3×3 matrix $\boldsymbol{T}(\Delta t; \omega, \nu, i, \lambda, \theta, \phi, r)$ performs the necessary rescalings and coordinate transformations.

Practical position observability can be characterized by the time histories of the along-track, cross-track, and altitude standard deviations, which are the square roots of the three diagonal elements of the $\boldsymbol{P}_{\mathrm{aca}}(\Delta t)$ covariance matrix. If these quantities are small throughout the data interval, $\Delta t_1 \leq \Delta t \leq \Delta t_K$, then the orbit and the spacecraft position can be observed practically.

Practical observability of the magnetometer biases, the external field coefficients, and the internal field coefficient perturbations can be tested using the original large $\boldsymbol{P}_p$ covariance matrix. If the standard deviation of a given quantity is small, that is, if the square root of the corresponding diagonal element of $\boldsymbol{P}_p$ is small, then the quantity can be observed practically with the given measurements.

B. Tracking Error Analysis

The net effects of all modeled error sources can be investigated by comparing truth model quantities to the corresponding estimates generated by the filter. The difference between the estimated value of any quantity and its corresponding truth model value is the "actual" estimation error for this quantity. In addition to random magnetometer measurement errors, this type of analysis includes the effects of nonlinearities, unestimated higher degree magnetic field terms, and celestial attitude measurement errors. As an additional check, the errors generated in this type of analysis can be compared to the standard deviations predicted by covariance analysis to verify its validity.

The estimation errors of various quantities have been examined. Position estimation error time histories have been computed in along-track/cross-track/altitude coordinates as seen from the truth model spacecraft position. Also computed have been magnetometer bias estimation errors, external field coefficient estimation errors, and estimation errors for the internal field coefficient perturbations.

V. Results and Discussion

A. Practical Observability as a Function of Orbit and Field Characteristics

The position variances, bias variances, and field coefficient variances have been examined for a number of different cases. Table 1 gives a summary of relevant standard deviations as they vary with orbit and field model. For all cases in Table 1, the number of samples $K = 2000$ and the sample spacing $\Delta t_{k+1} - \Delta t_k = 50$ s, which translates into 27.8 h of data. The drag effect for all of these cases is in the range 10^{-16} rad/s$^2 \leq M_2 \leq 10^{-13}$ rad/s^2. The three columns of Table 1 under the label "Maximum component σ" give the maxima over the data interval $\Delta t_1 \leq \Delta t \leq \Delta t_K$ of the predicted standard deviations of the along-track (AT), cross-track (CT), and altitude component errors.

In all cases except for the last line of the table, the analysis assumes that field coefficient perturbations are estimated up to degree and order 10; i.e., $N = 10$ is used in the filter. The last row examines the method's accuracy for a planet where the main dipole field is almost aligned with the axis of rotation, as on Saturn. The analysis assumes a dipole (first-degree) model aligned with the south pole: $g_1^0 = g_1^0$ of Earth and $g_1^1 = h_1^1 = 0$.

The last column of Table 1 has been included because it is representative of the standard deviations of other field model coefficients. In all cases considered so far, the standard deviations of some higher degree coefficients are larger than the standard deviation of Δg_1^0, but the sizes of the standard deviations of the higher degree terms are correlated with the size of the Δg_1^0 standard deviation. Similarly, the standard deviations of the external field coefficients are usually smaller than σ of Δg_1^0, but their changes in magnitude from case to case are correlated with σ of Δg_1^0.

The table demonstrates mathematical observability of the system in all cases except that of a circular orbit with zero inclination. The first six lines of Table 1 show how practical observability varies with orbital inclination for a nearly circular orbit. Observability of the field model coefficients is practically zero for $i \leq 10$ deg, as indicated in the last column, and along-track position becomes unobservable as the inclination goes to zero.

Lack of observability at zero orbital inclination and zero orbital eccentricity can be explained. For $i = 0$, the colatitude is constant at $\theta = \pi/2$ around the entire orbit. For a circular orbit, a/r is also a constant. These two effects combine to nullify the effect of degree, n, in the spherical harmonic field model expansion, Eqs. (3a–3c). The field's components around the orbit are simply periodic functions of longitude, ϕ, represented as Fourier series. The resulting periodic measurement time history contains no information about the relative importance of terms of different degree, and it contains no phase information relative to Earth, which leaves longitude (along-track position) unobservable.

A comparison between lines 1 and 7 of Table 1 shows the effect of altitude for nearly circular orbits. Line 7 corresponds to a mean semimajor axis of 1.5 Earth radii. The accuracy degrades somewhat for the higher altitude, probably because the absolute strength of the main dipole field has fallen off by 63% (as compared to line 1) due to the $1/r^3$ factor in the first-degree terms of Eqs. (3a–3c). The line-7 case may be near the maximum useful altitude for the technique. Field-producing external ring currents may exist above 2 Earth radii, but the filter assumes that the data come from locations of zero current.

Lines 8 and 9 are cases with significant eccentricity. Eccentricity is thought to improve observability of the field model coefficients. A comparison of the last column of lines 5 and 9 shows the truly beneficial effect of eccentricity on field model observability when inclination is low. This is made more noteworthy by the fact that line 9 has a higher average altitude, which otherwise would tend to increase uncertainty. Even though line 9 shows higher position standard deviations than line 5, the line-9 case is practically observable whereas the line-5 case is not. The enormous field model uncertainties on line 5 could swamp the entire filtering process, not even permitting convergence.

The last row of Table 1 shows that the observability of the system is not dependent on higher degree content in the field model (field "richness"), nor is it dependent on the cant of the magnetic poles with respect to Earth's rotation axis. The observability of the orbit for the case of field-magnitude-only filter innovations, the system tested in Ref. 5, is dependent both on field cant and on higher harmonic field model content.[11]

Detailed information about the predicted standard deviations is best presented in graphical form. For example, Fig. 1 presents three component standard deviations as functions of time. These time histories correspond to the first case in Table 1. The along-track standard deviation (solid line) is generally larger than the cross-track (dashed line) and altitude (dotted line) standard deviations, and it is slightly larger at the beginning and at the end of the data interval due to uncertainty in the estimated drag parameter M_2.

Standard deviations for the field coefficient uncertainties are shown in Fig. 2. These values also correspond to case 1 in Table 1. These standard deviations are plotted vs. their element number in the $\boldsymbol{p}$ estimation vector. Thus, the plotted points begin at horizontal axis value 11, the element number of q_1^0, and they end at value 139, the element number of h_{10}^{10}; cf. Eq. (1). The degree and order of the coefficients estimated in this case are 10. The standard deviations for elements 14–19, those corresponding to the secular rate terms $\dot{q}_1^0, \dot{q}_1^1, \dot{s}_1^1, \dot{g}_1^0, \dot{g}_1^1$, and $\dot{h}_1^1$, have been multiplied by the time length

Table 1 Standard deviation as measure of practical observability for various cases

Case	i, deg	Apogee altitude, km	Perigee altitude, km	Field model	Yaw maneuver, 90 deg	Maximum component σ AT, m	CT, m	Altitude, m	σ of Δg_1^0, nT
1	88.1	585	515	IGRF 1985	No	333.5	63.8	154.4	0.41
2	45.0	564	536	IGRF 1985	No	194.6	156.0	45.4	1.83
3	20.0	564	536	IGRF 1985	No	269.6	403.8	52.7	1.26×10^2
4	10.0	564	536	IGRF 1985	No	380.0	599.9	61.4	4.17×10^3
5	1.0	564	536	IGRF 1985	No	1831.8	734.2	68.2	4.06×10^8
6	0.2	564	536	IGRF 1985	No	7713.0	539.5	71.1	5.9×10^{11}
7	88.0	3199	3180	IGRF 1985	No	1398.7	274.0	662.8	1.17
8	88.0	3200	500	IGRF 1985	No	629.2	120.3	279.3	0.99
9	1.0	3200	500	IGRF 1985	Yes	2270.6	1339.1	153.3	8.24×10^3
10	88.5	551	549	Dipole ‖ South Pole	No	123.0	65.5	13.2	0.39

Table 2 Representative estimation errors for various cases

Case	i, deg	Apogee altitude, km	Perigee altitude, km	N Used in filter	Yaw maneuver, 90 deg	Maximum component errors			Δg_1^0 Error, nT
						AT, m	CT, m	Altitude, m	
1	88.1	585	515	10	No	208.1	35.1	93.6	−0.34
2	45.0	564	536	10	No	127.1	71.0	50.0	−4.21
3	20.0	557	543	10	No	427.6	244.5	66.8	1.87×10^2
4	10.0	557	543	10	No	826.1	1041.5	182.6	2.50×10^3
5	88.0	3199	3180	10	No	1416.5	486.9	362.9	0.34
6	1.0	3200	500	10	Yes	4376.7	1281.7	378.3	5.65×10^3
7	88.1	585	515	8	No	2473.3	317.6	1000.1	2.51

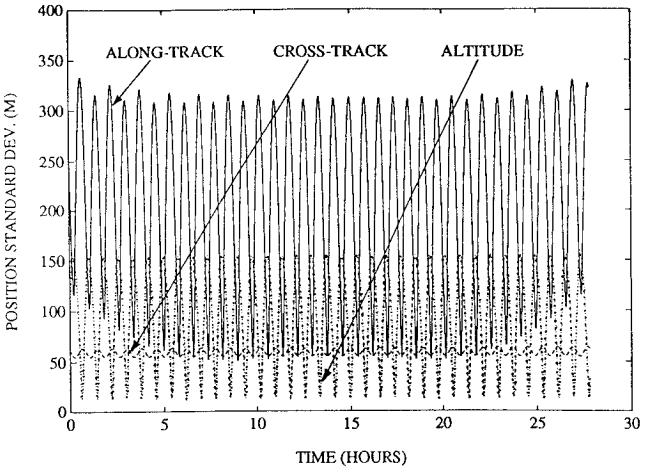

Fig. 1 Predicted standard deviation time histories for position component errors.

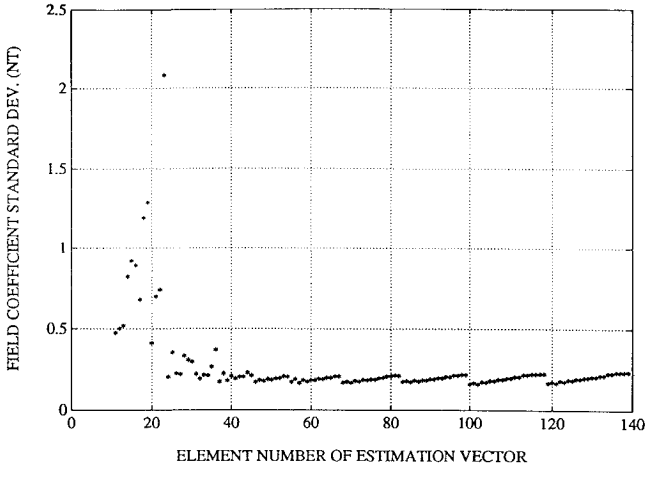

Fig. 2 Predicted standard deviations for field model coefficients.

of the available data, $\Delta t_K - \Delta t_1 = 99{,}950$ s, which gives their contribution to the field uncertainty at the end of the interval. Figure 2 indicates that this adapted filter could be used to determine Earth's magnetic field with respectable accuracy. Note that the method cannot distinguish between the main internal field and the static part of the induced internal field.

B. Errors Between Estimated and Truth Model Values

Truth-model-generated measurements have been run through the batch filter for a number of cases. Errors have been calculated for spacecraft position, for magnetometer biases, and for field model coefficients. Table 2 gives a summary of several cases, presenting representative estimation errors. Similar to the covariance analysis cases, each case in Table 2 uses $K = 2000$ samples and a sample spacing of $\Delta t_{k+1} - \Delta t_k = 50$ s. The three columns of Table 2 under the label "Maximum component errors" give the maxima over the data interval, $\Delta t_1 \leq \Delta t \leq \Delta t_K$, of the along-track (AT), cross-track (CT), and altitude component errors. Note that the case numbers in Table 2 do not exactly correspond to the case numbers in Table 1.

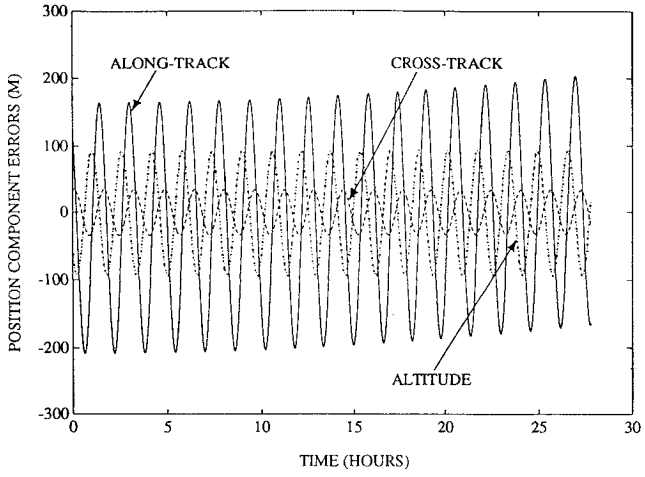

Fig. 3 Position component error time histories for inclined, low-altitude case.

The first thing to note about these results is the rough similarity between the error magnitudes in Table 2 and the corresponding standard deviations reported for similar cases in Table 1; cases 1–4 of Table 2 are similar to cases 1–4 of Table 1, and cases 5 and 6 of Table 2 are similar to cases 7 and 9 of Table 1. This implies that magnetometer random noise, the only uncertainty modeled in Table 1, is a principal cause of system inaccuracy. The additional uncertainties that affect the errors reported in cases 1–6 of Table 2, random attitude error and unmodeled 11th- to 13th-degree field effects, do not seem to make the actual errors much larger.

The effects of neglecting 9th- and 10th-degree terms in the filter's field model are demonstrated by cases 1 and 7 of Table 2. Case 1 includes these terms, and it estimates perturbations for these coefficients. Case 7 totally neglects these terms. The accuracy of case 7 is poorer by an order of magnitude or more. The filter must estimate field terms beyond eighth degree in order to achieve the best possible positional accuracy.

The estimation errors corresponding to case 1 are shown in more detail in Figs. 3–5. Figure 3 plots the three component errors vs time. Consistent with the modeled standard deviation time histories of Fig. 1, the along-track component (solid curve) is the largest source of position error. Also, the average value of along-track error wanders slightly during the filtering interval due to drag uncertainty. The total position error time history is plotted in Fig. 4. It is the Euclidean distance from the truth model spacecraft position to the estimated spacecraft position. Its peak value for this case is 209 m and its root-mean-square (rms) value is 150 m, which is sufficient accuracy for many spacecraft missions. Of all the cases, this one shows the best accuracy, probably because its orbit combines low altitude with high inclination.

The field model coefficient errors in Fig. 5 are similarly encouraging. The worst error is just under 1.5 nT. Also, the three magnetometer bias errors for this case, although not shown, are each less than 1.2 nT. Note that the horizontal axis in Fig. 5 has the same meaning as the horizontal axis in Fig. 2.

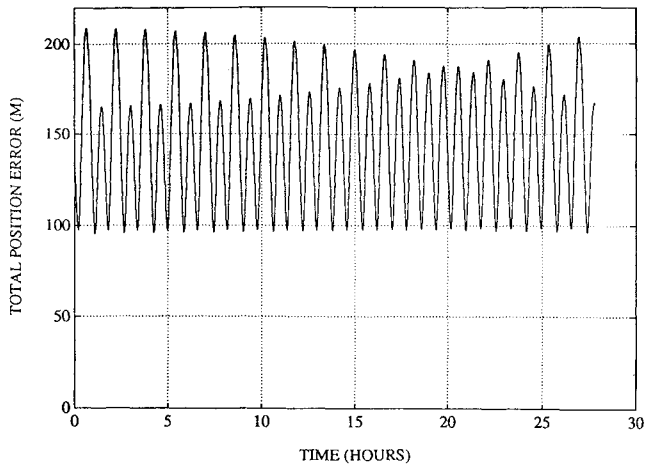

Fig. 4 Total position error time history for inclined, low-altitude case.

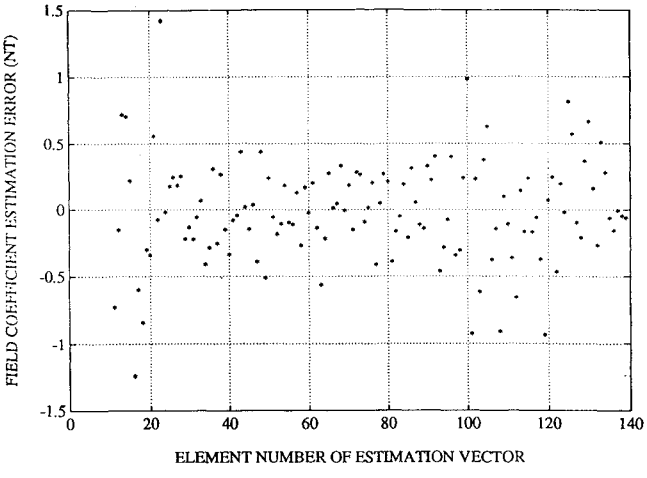

Fig. 5 Field model coefficient errors for inclined, low-altitude case.

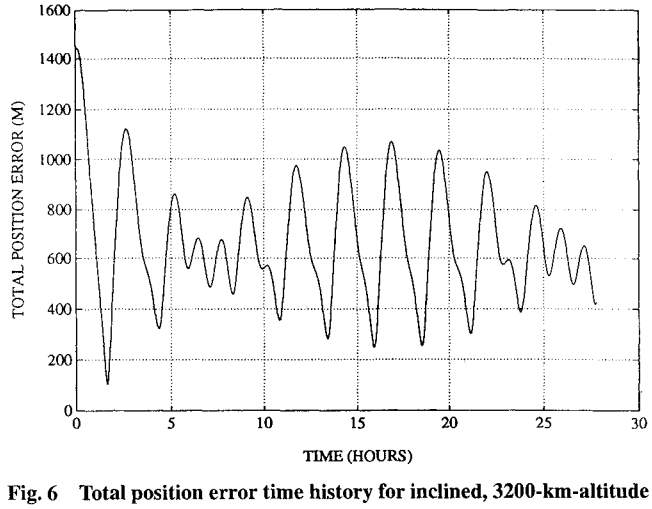

Fig. 6 Total position error time history for inclined, 3200-km-altitude case.

The total position error time history for a high-altitude, inclined, circular orbit is shown in Fig. 6. This is case 5 from Table 2. Consistent with the prediction based upon covariance analysis, accuracy is degraded due to the decreased field strength at a semimajor axis of 1.5 Earth radii. Nevertheless, the 1440 m peak error and the 700 m rms error are sufficiently accurate for some missions.

The results reported in Table 2 are affected by the choice of the random-number generator seed in the truth model. For example, a filter run has been made on a measurement data set whose only difference from case 1 of Table 2 is in the random-number sequence used to choose truth model field perturbations and attitude and magnetometer measurement errors. This run produced different numbers from those reported for the last four columns of case 1 in Table 2: 123.8 m maximum along-track error, 52.6 m maximum cross-track error, 35.4 m maximum altitude error, and $\Delta g_1^0 = 0.61$ nT. Although these changes are significant, they still correspond to levels predicted by the variances for case 1 of Table 1, and they still indicate excellent filter performance.

C. Comparison with Related Filters

As mentioned above, Psiaki et al.[5] have already tested a batch filter that operates only on the field magnitude and that estimates only the first 10 elements of the $\boldsymbol{p}$ vector defined in Eq. (1). It uses a 10th-degree IGRF field model with no corrective perturbations. In a representative case, the accuracy achieved by this filter using data from the DE-2 spacecraft was 18 km peak total position error.

To illustrate the improvements achieved with the present method, truth model magnetometer measurements for a case almost identical to case 1 of Table 2 have been filtered using the batch filter of Ref. 5. It achieves a maximum total position error of 33.4 km for this case, and the rms total position error is 20.0 km. The maximum component errors are 22.5 km along track, 27.2 km cross track, and 2.7 km altitude.

This accuracy is more than two orders of magnitude worse than for the presently proposed filter and is even worse than what was achieved for DE-2 in Ref. 5. One possible reason for poorer performance than on DE-2 is that the 1% truth model perturbations to the 1985 IGRF magnetic field may be larger than the actual field uncertainty for the DE-2 case. Langel has said privately that uncertainties of IGRF coefficients, even with secular propagation to a particular year, are likely to be less than min (0.5%, 50 nT). These uncertainties are about 50% smaller than the perturbations used in this study's truth model. Such a reduction in the field model uncertainty would account for the better performance of the actual DE-2 case in comparison to the simulated case reported here.

There are two differences between the present filter and the filter of Ref. 5: the use of star sensor attitude information and the estimation of field model coefficients. An investigation has been made to determine whether the addition of star sensor data alone could account for the improved filtering performance. This investigation filtered the truth model data corresponding to case 1 of Table 2 using a modified filter.

The modified filter is just like the filter described in Sec. II, except that only the first 10 elements of the $\boldsymbol{p}$ vector are estimated. The remaining are all assumed to be zero. Thus, the modified filter's only improvement over the filter of Ref. 5 is its use of attitude information.

The accuracy achieved by the modified filter is 9.5 km peak total position error and 4.4 km rms total position error. The component error maxima are 8.6 km along track, 4.5 km cross track, and 1.4 km altitude. These component error maxima are one-sixth to one-half of those for a similar case that used the filter of Ref. 5, but they are 15 to 127 times larger than the errors in case 1 of Table 2. Thus, the estimation of magnetic field model correction terms is a significant contributor to increased spacecraft positional accuracy.

D. Discussion

The accuracy capabilities being claimed for this new technique are on the order of 200 m for the best cases. This may seem unjustified because the orbital dynamics model used in the filter is accurate only to about 10 km for the filtering time spans envisioned. Thus, in its present form, this filter would probably produce positional errors on the order of 10 km when dealing with real flight data due to the limited fidelity of its orbital dynamics.

Radomski et al.[2] show that it is possible to propagate orbits for about a day to within an accuracy of about 50–100 m by using an orbital dynamics model that includes gravity terms beyond the J_2 term, the periodic effects of gravity and drag perturbations, a more detailed atmospheric drag model, solar and lunar effects, and direct numerical integration. Their scheme also estimates only one drag parameter. Their orbit propagation method could be directly incorporated into the present filter. This modification would increase the computational load, but it would also eliminate orbit propagation accuracy as a limiting factor for the technique. In the absence of other sources of modeling error, such changes would make the

filter capable of achieving its predicted 200-m accuracy level when working with real flight data from an accurate magnetometer and three-axis star sensor.

Additional possible sources of error that have not been considered are star sensor biases and star sensor/magnetometer misalignment. Perhaps such systematic error terms could be estimated. This issue should be addressed in the future.

A ridge-type filter might be used to alleviate the problem of unobservability when the spacecraft orbit has low inclination and low ellipticity. Ridge-type estimation techniques rely on a priori information when the system in question is unobservable or nearly so. Although the resulting estimate is biased, it can be superior to an unbiased estimate in cases of low observability if the ridge filter is properly tuned.[12] In the problem at hand, a ridge filter might use a priori information only for the field coefficient perturbations, not for the orbit parameters, the magnetometer biases, the external ring current parameters, or the secular field perturbations. This approach should enable estimation of circular, low-inclination orbits. Its accuracy in such cases is likely to be lower than what the basic filter could achieve for a spacecraft orbit with significant inclination.

A high level of sunspot activity results in an increase in the solar wind and a magnetic storm at Earth.[8] When this happens, the accuracy of the proposed method will be degraded by an unpredictable amount. The batch filter may be able to function fairly well starting about 24 h after the onset of a storm, during the final recovery phase, if its time-varying external ring current model captures most of the disturbance effects. This is another subject that deserves more investigation. Any meaningful investigation of this problem must involve real flight data from a magnetically active period, one in which Earth's main field is experiencing significant storm-induced perturbations.

Of course, the real proof of the achievable accuracy of this new technique will require filtering of actual flight data and comparison with precise tracking-station-derived position, similar to what was done in Ref. 5. There may be other unforeseen error sources, and real flight data will uncover any such surprises. Nevertheless, any surprises are unlikely to make the estimation vector unobservable. They would simply degrade accuracy.

E. Computational Experience

The computation time required by the algorithm is considerable. If all 10th-degree coefficient perturbations are estimated, then the dimension of the $\boldsymbol{p}$ estimation vector is 139. For this size estimation vector and $K = 2000$ sample points, the batch filter takes about 4 min per Gauss-Newton iteration on an HP (Apollo) 9000 model 720 workstation. This is a 1 Mflop workstation for double-precision arithmetic. For good first guesses the algorithm may converge in four iterations or fewer. For one case with a very poor first guess—the rms total position error between the true orbit and the guessed orbit was 2700 km—the filter required 25 iterations (100 min) to converge. This large computational load would make the method difficult to apply autonomously if the flight computer's speed were in the 10-Kflop range.

A recursive approach such as an extended Kalman filter might be a more efficient approach for on-board implementation of this orbit determination system. A recursive approach would save on memory and computation time per update, but it would have to include a process noise model that would need to be correctly tuned. If implemented properly, a recursive implementation of this orbit determination scheme should yield accuracies comparable to those achieved in the present study by the batch filter. A recursive filter has not been used in the present study for the sake of simplicity; the goal of this study has been to demonstrate observability and expected performance, not to achieve the most efficient possible on-board implementation.

VI. Conclusions

A standard batch filter has been adapted for near-Earth autonomous orbit determination by use of an unusual estimation vector and unusual measurements. It simultaneously estimates the spacecraft orbit, magnetometer biases, and refinements to a model of Earth's magnetic field. It requires measurement time histories from a three-axis magnetometer and from a three-axis star sensor system. It performs its task using these measurements together with a spherical harmonic expansion of Earth's magnetic field and an orbit propagation routine.

The orbit and the field model are simultaneously observable except in orbits with zero inclination and zero eccentricity. This simulation study assumes that the magnetometer accuracy, excluding biases, is 10 nT, that the star sensor accuracy is 2 arcsec per axis with no biases, that accurate orbit propagation can be performed using a constant drag coefficient, and that no magnetic storm corrupts the data. For inclinations above 45 deg and altitudes of about 500 km, the simulation results predict a system accuracy on the order of 200 m when processing 2000 data points evenly spaced over 28 h. Field model coefficient accuracy on the order of 1 nT is predicted for inclinations near 90 deg and an altitude of 500 km.

VII. Appendix: Orbital Dynamics Model

The following orbital dynamics model is used by the filter to determine spacecraft position as a function of the first seven elements of the $\boldsymbol{p}$ estimation vector, M_0, M_1, M_2, e, ω_0, λ_0, i. This model has been borrowed directly from Ref. 5. Note that an Earth rotation rate term was erroneously omitted from Eq. (24c) of Ref. 5; it now appears in Eq. (A7c) below.

The position calculations determine the mean semimajor axis $\bar{a}$ after calculating two intermediate quantities, a_M and a_0:

$$a_M = [806.81359 M_1]^{-2/3} \tag{A1}$$

$$a_0 = a_M \left[1 + \frac{0.75 J_2 (3\cos^2 i - 1)}{a_M^2 (1 - e^2)^{3/2}} \right]^{2/3} \tag{A2}$$

$$\bar{a} = a_0 \left[1 - \frac{0.75 J_2 (3\cos^2 i - 1)}{a_M^2 (1 - e^2)^{3/2}} \right] \tag{A3}$$

where M_1 is in units of radians per second and $\bar{a}$, a_M, and a_0 are all in units of Earth radii. Next comes a calculation of the secular effects of J_2 on the rates of change of the argument of perigee and the longitude of the ascending node:

$$\omega' = \frac{0.75 J_2 (5\cos^2 i - 1)}{a_0^2 (1 - e^2)^2} \tag{A4}$$

$$\Omega' = \frac{-1.5 J_2 \cos i}{a_0^2 (1 - e^2)^2} \tag{A5}$$

where ω' and Ω' are both in units of radians per radian of mean motion. The decay rate of the mean semimajor axis due to drag is modeled as

$$\dot{a} = -\frac{4}{3} \bar{a} \frac{M_2}{M_1} \tag{A6}$$

The model includes time variations of four Keplerian elements. These are propagated from epoch to time Δt as follows:

$$M = M_0 + M_1 \Delta_t + M_2 \Delta t^2 \tag{A7a}$$

$$\omega = \omega_0 + \omega' \left(M_1 \Delta t + M_2 \Delta t^2 \right) \tag{A7b}$$

$$\lambda = \lambda_0 + \Omega' \left(M_1 \Delta t + M_2 \Delta t^2 \right) - \omega_e \Delta t \tag{A7c}$$

$$a = \bar{a} + \dot{a} \Delta t \tag{A7d}$$

The remaining two Kepler elements, e and i, are assumed to remain constant. Note that ω_e in Eq. (A7c) is Earth's rotation rate with respect to inertial coordinates.

The dynamic model finishes the position determination by numerically solving Kepler's equation for the eccentric anomaly E:

$$M - E + e \sin(E) = 0 \tag{A8}$$

then computing the true anomaly

$$\nu = \tan^{-1} \frac{\sqrt{1 - e^2} \sin E}{\cos E - e} \tag{A9}$$

and the position

$$\theta(\Delta t;\ M_0,\ M_1,\ M_2,\ e,\ \omega_0,\ \lambda_0,\ i) = \cos^{-1}[\sin(\omega + \nu)\sin i] \tag{A10a}$$

$$\phi(\Delta t;\ M_0,\ M_1,\ M_2,\ e,\ \omega_0,\ \lambda_0,\ i) = \tan^{-1}\frac{\sin\lambda\cos(\omega+\nu) + \cos\lambda\sin(\omega+\nu)\cos i}{\cos\lambda\cos(\omega+\nu) - \sin\lambda\sin(\omega+\nu)\cos i} \tag{A10b}$$

$$r(\Delta t;\ M_0,\ M_1,\ M_2,\ e,\ \omega_0,\ \lambda_0,\ i) = R_E a(1 - e\cos E) \tag{A10c}$$

where R_E is Earth's mean equatorial radius ($=6378.14\times10^3$ m). The batch filter also requires partial derivatives of θ, ϕ, and r with respect to M_0, M_1, M_2, e, ω_0, λ_0, and i, which are calculated analytically via successive differentiation of Eqs. (A1–A10c).

This dynamic model includes only the secular effects of J_2, not the periodic effects. It has some of the secular effects of drag, but not the secular decay of eccentricity due to drag. It can have an inaccuracy on the order of 10 km for position propagation over a 1-day interval. Nevertheless, this model is adequate for the purpose of studying the observability and accuracy of the proposed batch filter orbit determination system.

Acknowledgment

Robert A. Langel of NASA Goddard Spaceflight Center provided helpful information and suggestions during several phone conversations with the author.

References

[1]Russell, C. T., "Planetary Magnetism," *Geomagnetism*, edited by J. A. Jacobs, Vol. 2, Academic, New York, 1987, pp. 457–524.

[2]Radomski, M. S., Davis, B. E., Samii, M. V., Engel, C. J., and Doll, C. E., "Evaluation of Advanced Geopotential Models for Operational Orbit Determination," NASA CP-3011, May 1988, pp. 595–612.

[3]Chory, M. A., Hoffman, D. D., and LeMay, J. L., "Satellite Autonomous Navigation: Status and History," *Proceedings of the IEEE Position, Location, and Navigation Symposium*, Institute of Electrical and Electronic Engineers, New York, 1986, pp. 110–121.

[4]Tai, F., and Noerdlinger, P. D., "A Low Cost Autonomous Navigation System," *Guidance and Control 1989; Proceedings of the Annual Rocky Mountain Guidance and Control Conference* (Keystone, CO), 1989, pp. 3–23; also American Astronautical Society Paper 89-001.

[5]Psiaki, M. L., Huang, L., and Fox, S. M., "Ground Tests of Magnetometer-Based Autonomous Navigation (MAGNAV) for Low-Earth-Orbiting Spacecraft," *Journal of Guidance, Control, and Dynamics*, Vol. 16, No. 1, 1993, pp. 206–214.

[6]Shorshi, G., and Bar-Itzhack, I. Y., "Satellite Autonomous Navigation Based on Magnetic Field Measurements," *Proceedings of the AAS/GSFC International Symposium on Space Flight Dynamics* (Greenbelt, MD), 1993; also American Astronautical Society Paper 93-255.

[7]Langel, R. A., "The Main Field," *Geomagnetism*, edited by J. A. Jacobs, Vol. 1, Academic, New York, 1987, pp. 249–512.

[8]Wertz, J. R. (ed.), *Spacecraft Attitude Determination and Control*, Reidel, Boston, MA, 1978.

[9]Gill, P. E., Murray, W., and Wright, M. H., *Practical Optimization*, Academic, New York, 1981.

[10]Langel, R., Berbert, J., Jennings, T., and Horner, R., "MAGSAT Data Processing: A Report for Investigators," NASA TM-82160, Nov. 1981.

[11]Psiaki, M. L., and Martel, F., "Autonomous Magnetic Navigation for Earth Orbiting Spacecraft," *Proceedings of the Third Annual AIAA/USU Conference on Small Satellites*, Utah State Univ. Publications (Logan, UT), 1989.

[12]Cicci, D. A., and Tapley, B. D., "Optimal Solutions of Unobservable Orbit Determination Problems," *Celestial Mechanics*, Vol. 44, No. 4, 1988, pp. 339–363.